# Self-Assembly of "Paint-On" Colloidal Crystals Using Poly(styrene-*co*-*N*-isopropylacrylamide) Spheres

Jonathan G. McGrath,[†] Robert D. Bock,[‡] J. Michael Cathcart,[‡] and L. Andrew Lyon*[,†]

*School of Chemistry and Biochemistry and Petit Institute for Bioengineering and Bioscience, Georgia Institute of Technology, Atlanta, Georgia 30332-0400, and Electro-Optical Systems Laboratory, Georgia Tech Research Institute, Atlanta, Georgia 30332-0834*

*Received August 16, 2006. Revised Manuscript Received January 31, 2007*

We report on the synthesis of monodispersed, spherical colloidal particles composed of poly(styrene-*co*-*N*-isopropylacrylamide) (pS-*co*-NIPAm) that rapidly self-assemble via simple solvent evaporation to form 3-D colloidal crystals that are both robust and uniformly diffractive. As a suspension of the pS-*co*-NIPAm particles dries, the interactions of their soft, flexible peripheries assist in particle self-assembly to form a close-packed ordered structure. Interparticle adhesion occurs at these contacts as the final amount of solvent evaporates, enhancing the durability of the assembly. The dense core provides stability of the ordered structure subsequent to drying. These dried, crystalline films exhibit Bragg diffraction, which can be modified by changing the particle size through varying the monomer feed concentrations. The facile drying process used for crystalline assembly presents a unique approach to photonic inks that can be used as "paint-on" (i.e., processable) dispersions, which are advantageous for the fabrication of materials for optical applications.

## Introduction

Monodispersed, spherical particles have been investigated extensively for their use in the fabrication of colloidal crystals for the design of optical materials.[1] For example, ordered structures such as these have even been shown to exhibit photonic band gap behavior.[2,3] The investigation of these materials has established their use in many optical applications, such as waveguides,[4,5] filters, switches, and sensing devices.[6,7] To produce colloidal crystals that can achieve these functions, it is necessary to maintain control over the assembly of the particles to afford reproducibility and to minimize structural defects that can diminish the optical properties of the material. Self-assembly approaches offer a distinct advantage in that they are efficient, require minimal fabrication efforts, and can be easily modified for widespread manufacturing purposes. However, such approaches are intrinsically tied to obtaining thermodynamic control over assembly, which often requires very slow assembly or sedimentation to limit the number and size of kinetically trapped defects. A self-assembly technique that is appropriate for creating processable materials should be quick, simple, and provide a crystalline construct that possesses a high degree of stability, so that it will be useful for many optical applications.[8,9] A simple technique that uses a highly processable photonic precursor that can be applied as a paint to form an intended structure would be particularly advantageous.

Many types of self-assembly based fabrication strategies have been explored to produce colloidal crystals. Some of the simplest techniques include sedimentation and centrifugation procedures. However, slow sedimentation is time-consuming, and rapid centrifugation can cause defects that disrupt the crystalline order. Many diverse methods have been investigated to enhance the speed of crystal formation through controlled processes. Capillary deposition,[10] vertical deposition,[11,12] convective assembly,[13] spin-coating,[14] electrophoretic assembly,[15,16] and other innovative designs[17,18] have been investigated for the purposes of controlling the extent and orientation of crystalline order, as well as crystal thickness. However, these methods often require complex configurations or long deposition times that are essential for crystal formation. Simple methods that make use of solvent

* To whom correspondence should be addressed. E-mail: LL62@mail.gatech.edu.
[†] Georgia Institute of Technology.
[‡] Georgia Tech Research Institute.

(1) Xia, Y.; Gates, B.; Yin, Y.; Lu, Y. *Adv. Mater.* **2000**, *12*, 693−713.
(2) Joannopoulos, J. D.; Villeneuve, P. R.; Fan, S. *Nature* **1997**, *387*, 830.
(3) Yablonovitch, E. *J. Opt. Soc. Am. B* **1993**, *10*, 283−295.
(4) Lee, W.; Pruzinsky, S. A.; Braun, P. V. *Adv. Mater.* **2002**, *14*, 271−274.
(5) Li, J.; Herman, P. R.; Valdivia, C. E.; Kitaev, V.; Ozin, G. A. *Opt. Express* **2005**, *13*, 6454−6459.
(6) Holtz, J. H.; Asher, S. A. *Nature* **1997**, *389*, 829−832.
(7) Ben-Moshe, M.; Alexeev, V. L.; Asher, S. A. *Anal. Chem.* **2006**, *78*, 5149−5157.
(8) Norris, D. J.; Arlinghaus, E. G.; Meng, L.; Heiny, R.; Scriven, L. E. *Adv. Mater.* **2004**, *16*, 1393−1399.
(9) Xia, Y.; Gates, B.; Li, Z.-Y. *Adv. Mater.* **2001**, *13*, 409−413.
(10) Li, H.-L.; Marlow, F. *Chem. Mater.* **2006**, *18*, 1803−1810.
(11) Jiang, P.; Bertone, J. F.; Hwang, K. S.; Colvin, V. L. *Chem. Mater.* **1999**, *11*, 2132−2140.
(12) Li, J.; Han, Y. *Langmuir* **2006**, *22*, 1885−1890.
(13) Wostyn, K.; Zhao, Y.; Yee, B.; Clays, K.; Persoons, A.; De Schaetzen, G.; Hellemans, L. *J. Chem. Phys.* **2003**, *118*, 10752−10757.
(14) Jiang, P.; McFarland, M. J. *J. Am. Chem. Soc.* **2004**, *126*, 13778−13786.
(15) Trau, M.; Saville, D. A.; Aksay, I. A. *Science* **1996**, *272*, 706−709.
(16) Rogach, A. L.; Kotov, N. A.; Koktysh, D. S.; Ostrander, J. W.; Ragoisha, G. A. *Chem. Mater.* **2000**, *12*, 2721−2726.
(17) Park, S. H.; Xia, Y. *Langmuir* **1999**, *15*, 266−273.
(18) Wong, S.; Kitaev, V.; Ozin Geoffrey, A. *J. Am. Chem. Soc.* **2003**, *125*, 15589−98.

10.1021/cm061931y CCC: $37.00 
Published on Web 03/06/2007

evaporation have also been explored, and the dynamics of these assembly interactions has been widely investigated.[19−21] These previously reported evaporation techniques provide the basis for designing a model scheme for quick crystal formation that can be adapted toward "paint-on" approaches.

It is interesting to note that mainly hard sphere systems have been used in the approaches described previously. Alternatively, crystals composed of soft colloidal spheres offer distinct properties that arise from the flexible polymer components.[22−25] The Lyon group has investigated colloidal crystals comprised of spherical hydrogel particles composed of poly-*N*-isopropylacrylamide (pNIPAm) that exhibit these types of soft interactions.[26,27] These particles can be assembled and the crystals subsequently annealed by means of the thermoresponsive property of the pNIPAm.[28] Particles composed of pNIPAm undergo a volume phase transition at ∼31 °C, such that the particle size decreases at high temperatures. Thermal annealing of concentrated solutions of pNIPAm particles allows for particle self-assembly as the particles return to their swollen state. This procedure presents a convenient method for rapid fabrication of crystalline materials, and the soft particle construct additionally enables simple adjustment of optical properties by varying the polymer volume fractions.[29] Furthermore, others have shown that dispersions of pNIPAm particles can also be used as "inks" to create 2-D self-assembled arrays formed by capillary forces during solvent evaporation, demonstrating the utility of the hydrogel character of the particles.[30]

Modifications to 3-D colloidal crystal systems have also been employed to effectively "glue" ordered particles together using polymeric hydrogels, which has given rise to tunable crystals that possess enhanced stability.[31,32] However, since these materials are composed of hydrogels, the crystals cannot be produced as dried, freestanding materials such as those obtainable from hard spheres. An attractive scheme for colloidal crystal formation can be realized by taking advantage of particles that possess two beneficial properties: soft interactions for particle assembly and hard sphere properties that enhance crystalline stability.[33]

In this work, we have synthesized spherical nanoparticles composed of poly(styrene-*co*-*N*-isopropylacrylamide (pS-*co*-NIPAm) that can be used to obtain robust, 3-D colloidal crystalline materials via the facile method of solvent evaporation under ambient conditions. Similar types of pS-*co*-NIPAm particles have been synthesized by the Hellweg group, which have also demonstrated ordered structures upon drying.[34] However, the pS-*co*-NIPAm particles that were used in the studies presented below do not exhibit thermoresponsivity due to the low concentrations of NIPAm used in the particle synthesis. The addition of NIPAm to the synthesis apparently only adds soft, hydrogel-like qualities that provide particle flexibility, but not thermoresponsivity. This distinctive characteristic appears to be a significant factor in the self-assembly of pS-*co*-NIPAm particles, whereby the soft particle exterior affects the interactions between neighboring particles during the drying process. As a sessile drop of an aqueous suspension of pS-*co*-NIPAm particles dries, the particles come into close contact and rearrange to form a "soft" crystalline phase, where the swollen particle peripheries interact repulsively in a manner similar to traditional hydrogel particle assemblies.[26,27] This attribute provides ample deformation at the particle periphery to allow for the formation of an ordered structure. As the final amount of solvent evaporates from the polymer, the particle size decreases due to deswelling; however, the crystalline order is retained due to interparticle contacts that become adhesive during drying. This crystalline order is then maintained by the dense polystyrene core, ultimately affording a stable, ordered configuration. These copolymer characteristics make these particles ideal for the formation of "paint-on" colloidal crystals.

## Experimental Procedures

**Materials.** The monomer *N*-isopropylacrylamide (NIPAm, Aldrich) was purified via recrystallization from hexane (J. T. Baker). Styrene, *N*,*N*′-methylenebis(acrylamide) (BIS), and ammonium persulfate (APS) were purchased from Aldrich and used as received. Distilled water was purified with a Barnstead E-Pure system to a resistance of 18 MΩ and then filtered through a 0.2 $\mu$m filter to remove particulate matter.

**Particle Synthesis.** Poly(styrene-*co*-*N*-isopropylacrylamide) (pS-*co*-NIPAm) particle synthesis was performed using a one-pot, surfactant-free emulsion polymerization adapted from the syntheses reported by the Hellweg group.[34] The monomer feed concentrations for pS-*co*-NIPAm synthesis contained either 73 or 75 mol % styrene to obtain particles with negligible thermoresponsivity (vide infra). Two batches of particles were prepared having different total monomer concentrations (280 and 500 mM) to obtain particles with different sizes. For the 280 mM monomer feed, 0.0204 mol of styrene (73 mol %), 0.0072 mol of NIPAm (26 mol %), and 0.0003 mol of BIS (1 mol %) were used. For the 500 mM monomer feed, 0.0375 mol of styrene (75 mol %), 0.0119 mol of NIPAm (24 mol %), and 0.0005 mol of BIS (1 mol %) were used. For both syntheses, NIPAm and BIS were dissolved in 100 mL of water, and the reaction mixture was heated to 70 °C and purged with nitrogen gas for 75 min in a three-necked round-bottomed flask equipped with a condenser and inlet for nitrogen with constant stirring. The styrene was added just prior to initiation. Initiation was performed using 0.027 mmol of APS for the 280 mM synthesis and 0.031 mmol of APS for the 500 mM synthesis, which was

(19) Okubo, T.; Kimura, K.; Kimura, H. *Colloid Polym. Sci.* **2002**, *280*, 1001−1008.
(20) Koh, Y. K.; Wong, C. C. *Langmuir* **2006**, *22*, 897−900.
(21) Juillerat, F.; Bowen, P.; Hofmann, H. *Langmuir* **2006**, *22*, 2249−2257.
(22) Senff, H.; Richtering, W. *J. Chem. Phys.* **1999**, *111*, 1705−1711.
(23) Hellweg, T.; Dewhurst, C. D.; Bruckner, E.; Kratz, K.; Eimer, W. *Colloid Polym. Sci.* **2000**, *278*, 972−978.
(24) Hu, Z.; Lu, X.; Gao, J. *Adv. Mater.* **2001**, *13*, 1708−1712.
(25) Alsayed, A. M.; Islam, M. F.; Zhang, J.; Collings, P. J.; Yodh, A. G. *Science* **2005**, *309*, 1207−1210.
(26) Debord, J. D.; Lyon, L. A. *J. Phys. Chem. B* **2000**, *104*, 6327−6331.
(27) Lyon, L. A.; Debord, J. D.; Debord, S. B.; Jones, C. D.; McGrath, J. G.; Serpe, M. J. *J. Phys. Chem. B* **2004**, *108*, 19099−19108.
(28) Pelton, R. *Adv. Colloid Interface Sci.* **2000**, *85*, 1−33.
(29) Debord, S. B.; Lyon, L. A. *J. Phys. Chem. B* **2003**, *107*, 2927−2932.
(30) Tsuji, S.; Kawaguchi, H. *Langmuir* **2005**, *21*, 8439−8442.
(31) Asher, S. A.; Holtz, J.; Liu, L.; Wu, Z. *J. Am. Chem. Soc.* **1994**, *116*, 4997−4998.
(32) Weissman, J. M.; Sunkara, H. B.; Tse, A. S.; Asher, S. A. *Science* **1996**, *274*, 959−960.
(33) Kalinina, O.; Kumacheva, E. *Macromolecules* **1999**, *32*, 4122−4129.
(34) Hellweg, T.; Dewhurst, C. D.; Eimer, W.; Kratz, K. *Langmuir* **2004**, *20*, 4330−4335.

pre-dissolved in 0.5 mL of water. Additional amounts of APS (0.044 mmol) were added to each synthesis 4 h after initiation to ensure reaction completion. After both reactions were allowed to react for 23 h, the reaction solutions were filtered using Whatman filter paper (No. 2) to remove any coagulum and cleaned by centrifugation 3 times for approximately 30 min at 15 400 relative centrifual force (rcf) at 25 °C to remove any unreacted monomer or oligomeric species, using distilled, deionized water for resuspension of the pellet.

**Photon Correlation Spectroscopy.** Hydrated particle sizes were determined using photon correlation spectroscopy (PCS, Protein Solutions, Inc.) equipped with an integrated Peltier temperature control device (±0.1 °C) using dilute solutions of pS-*co*-NIPAm particles (∼1−2.5 $\mu$g/mL). The average hydrodynamic radius ($R_h$) for each set of particles was calculated from the diffusion coefficient using the Stokes−Einstein equation. The sample was allowed to equilibrate at the appropriate temperature for 10 min before data collection. Scattered light from the fiber-coupled diode laser (798 nm) was collected at 90° with a fiber-coupled avalanche photodiode detector connected to a 248-channel autocorrelator board. The data were analyzed with Dynamics Software Version 5.20.05 (Protein Solutions, Inc.) using the Cumulants method for monomodal (Gaussian) size distribution analysis, and five measurements were obtained for statistical analysis of the $R_h$. Each measurement consisted of 5 data points, each collected using an acquisition (integration) time of 60 s.

**Static Light Scattering.** Multi-angle laser light scattering (MALLS, Wyatt Technology, Inc.) was employed to determine the radius of gyration ($R_g$) of the hydrated particles. Asymmetric field flow fractionation (AFFF, Eclipse, Wyatt Technology, Inc.) was utilized to achieve particle separation based on hydrodynamic volume using a solvent cross-flow.[35,36] The AFFF method that was employed first concentrated the sample at one end of the AFFF channel using the focusing mode, followed by sample elution using a cross-flow rate of 0.25 mL/min that decreased consistently over a period of 36 min, followed by an additional elution time of 20 min with no cross-flow. Particle elution continued to the MALLS detector, which was equipped with a Peltier device to maintain a flow-cell temperature of 25 °C. Scattered light from a GaAs laser operating at 684 nm was collected at 16 fixed angle detectors, and ASTRA 5.1.5.0 software was used to determine $R_g$ values using the Debye fit method. Samples were diluted as necessary to achieve appropriate light scattering signals following the AFFF separation. Uncertainty in calculated $R_g$ values was determined from the standard deviations of each slice of data in the Debye plot, using the ASTRA software.

**Transmission Electron Microscopy.** The particle size and interparticle interactions of dried pS-*co*-NIPAm particles were examined using transmission electron microscopy (TEM). Drops of dilute solutions of particles were placed on TEM copper grids (either Formvar or Carbon-B Type, 200 mesh, Ted Pella, Inc.) leaving at least one drop to dry overnight. A JEOL 100CX II instrument operating at 100 kV was used for TEM characterizations. Particle size distributions were calculated using ImageJ software.[37]

**Crystal Sample Preparation.** Dried crystals were prepared by spreading a drop of a concentrated pS-*co*-NIPAm aqueous suspension on a glass cover slip (VWR, 22 mm × 30 mm) using a plastic transfer pipet, to encompass an area of approximately 2 cm in diameter. These colloidal suspensions possessed polymer concentrations of 10 mg/mL for the 280 mM pS-*co*-NIPAm particles and 26 mg/mL for the 500 mM pS-*co*-NIPAm particles. The sessile drop was allowed to dry open to the atmosphere, which occurred after 60−90 min at ambient temperature. This sample preparation was used to prepare samples for SEM and reflectance spectroscopy characterizations.

**Optical Spectroscopy.** Reflectance spectroscopy of dried films was performed using a Cary 500 double beam scanning spectrophotometer (UV−vis−-NIR) operating in the spectral range of 175−3300 nm using an integrating sphere accessory and the accompanying WinUV software and scan package. Specular reflectance (or % reflectance) was determined indirectly by subtracting the diffuse reflectance from the total reflectance (specular + diffuse) at near-normal incidence. In situ reflectance spectra were collected during the drying process using a fiberoptic spectrophotometer (Ocean Optics, Inc., USB2000 with integrated OFLV-3 detector) and OOIBase32 software. A bifurcated source and detector fiber optic reflectance probe (R400−-7-vis/NIR) was employed by positioning the probe above the sample at near-normal incidence. A dark spectrum was obtained by covering the reflectance probe using the probe cap, and a 100% reflectance reference was obtained using a diffuse reflectance standard. The diameter of the reflectance probe optical fiber was 400 $\mu$m, which allowed for the interrogation of a wide sampling area during in situ drying experiments.

**Scanning Electron Microscopy.** A Hitachi S800 field emission gun scanning electron microscope operating at 10 kV was used to characterize the structural properties of dried samples of pS-*co*-NIPAm particles. Scanning electron microscopy (SEM) samples were prepared by drying a concentrated suspension of particles on a glass cover slip, onto which a 5 nm gold film was added using a Denton Vacuum Evaporator (DV-502A) equipped with an Inficon deposition monitor. Samples were placed on a flat, cylindrical specimen mount for imaging the top of the dried sample. To obtain images of sample cross-sections, a drop of the particle suspension was dried on a scored glass cover slip. After the sample dried completely, the cover slip was broken along a scored line, followed by deposition of a gold film, as described previously. A 45° specimen mount was used for obtaining images of the crystal cross-section by tilting the sample relative to the incident electron beam.

## Results

Two different sizes of pS-*co*-NIPAm particles, with slightly different co-monomer compositions, were synthesized by varying monomer feed concentrations (280 and 500 mM) and were used separately for the fabrication of dried colloidal crystals. Note that the 280 mM particles were synthesized using a feed of 73% styrene, 26% NIPAm, and 1% BIS, while the 500 mM particles were prepared from 75% styrene, 24% NIPAm, and 1% BIS. For simplicity, we will refer to the two batches of particles by the total monomer concentration designations (280 or 500 mM). However, the reader should be reminded that the smaller particles contain relatively ∼2% more NIPAm and ∼2% less styrene than the larger particles; this apparently subtle difference has a measurable impact on the particle structure and crystal assembly.

Photon correlation spectroscopy and multi-angle laser light scattering were used to determine the particle size when fully hydrated at 25 °C. The hydrodynamic radius ($R_h$) and radius of gyration ($R_g$) for each pS-*co*-NIPAm sample are listed in Table 1. The ratio of $R_g$ to $R_h$ is also listed; this factor can be used to characterize the radial mass distribution, or

(35) Wyatt, P. J.; Villalpando, D. N. *Langmuir* **1997**, *13*, 3913−3914.
(36) Andersson, M.; Wittgren, B.; Wahlund, K. G. *Anal. Chem.* **2001**, *73*, 4852−4861.
(37) Rasband, W. S. *ImageJ*; National Institutes of Health: Bethesda, MD, 1997−2004; http://rsb.info.nih.gov/ij/.

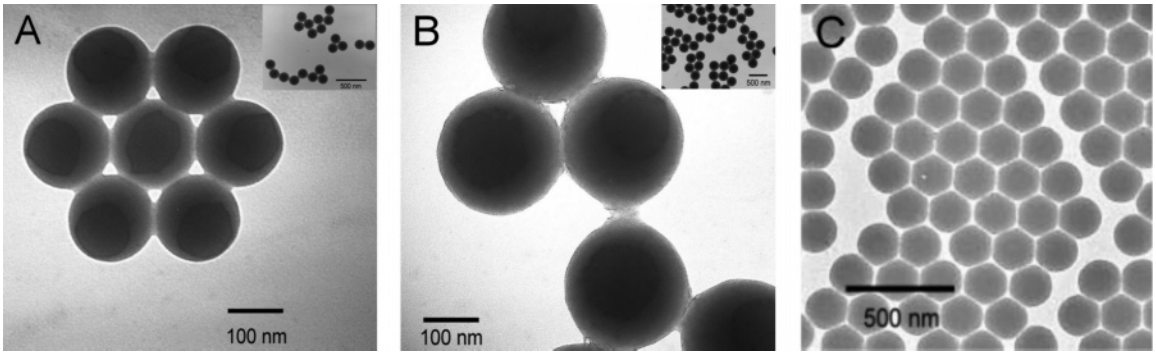


**Figure 1.** Transmission electron microscopy images of 280 mM pS-*co*-NIPAm nanoparticles (A) and 500 mM pS-*co*-NIPAm nanoparticles (B). Inset scale bar is 500 nm. Variations in particle morphology due to interparticle compression can be observed using a higher concentration of 500 mM pS-*co*-NIPAm particles to prepare the sample (C).

**Table 1. Particle Size Characterizations**[a]

| | MALLS $R_g$ (nm) | PCS $R_h$ (nm) | $R_g/R_h$ | TEM diameter (nm) |
|---|---|---|---|---|
| 280 mM pS-*co*-pNIPAm | 87.8 (0.3%) | 139.2 (±2.2) | 0.631 | 202.7 (±4.9) |
| 500 mM pS-*co*-pNIPAm | 124.4 (0.2%) | 159.0 (±1.2) | 0.782 | 268.1 (±6.6) |

[a] Standard deviations (±) and relative uncertainties (%) are noted in parentheses.

polymer chain segment density, in the particles. The particle diameter was determined using TEM to demonstrate the dried particle size that results from sample evaporation. The 280 mM pS-*co*-NIPAm particles were determined to have a diameter of 202.7 ± 4.9 nm ($n = 118$), while the 500 mM pS-*co*-NIPAm particles possess a diameter of 268.1 ± 6.6 nm ($n = 56$), both in their fully dried state.

The morphology of the dried pS-*co*-NIPAm particles is shown in Figure 1. Transmission electron microscopy images of dilute solutions of 280 mM pS-*co*-NIPAm (Figure 1A) and 500 mM pS-*co*-NIPAm (Figure 1B) seem to suggest that an adhesive interaction occurs at the interparticle contacts. A 2-D array of 500 mM pS-*co*-NIPAm particles was formed using a more concentrated solution for the sample preparation (Figure 1C). This image shows a somewhat different variation in the particle morphology when more particles are present. The particle shape appears to become less spherical as the particles are forced together into a dense array. Together, these results apparently suggest that the particle peripheries are somewhat soft and amenable to stretching/adhesion (Figure 1A,B) or compression (Figure 1C).

Dried colloidal crystals were fabricated by placing a drop of a pS-*co*-NIPAm particle suspension on a glass cover slip and allowing it to dry completely under ambient conditions. The resulting diffraction color is clearly shown in Figure 2. The 280 mM pS-*co*-NIPAm particles dry to a blue crystal, while the 500 mM pS-*co*-NIPAm particles produce a red crystalline film. This diffractive color is consistent across the entire sample, suggesting a high quality of uniform crystalline order. Although complete drying of these particular samples required approximately 60−90 min, spreading the drop over a larger area can reduce this drying time by increasing the rate of evaporation.[38,39]

Reflectance spectroscopy was employed to determine the wavelength of Bragg diffraction[27] for these crystalline

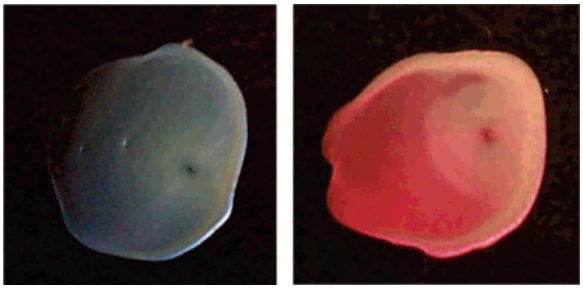

**Figure 2.** Digital camera images of the dried crystalline films formed through solvent evaporation of an aqueous suspension of pS-*co*-NIPAm particles. Left: crystal formed using 280 mM pS-*co*-NIPAm. Right: crystal formed using 500 mM pS-*co*-NIPAm particles.

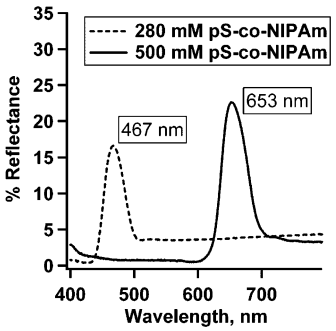


**Figure 3.** Reflectance spectra of colloidal crystals formed from pS-*co*-NIPAm particles.

materials at near-normal incidence. Dried colloidal crystals composed of 280 or 500 mM pS-*co*-NIPAm particles exhibit first-order Bragg diffraction at 467 and 653 nm, respectively (Figure 3). These diffraction wavelengths are consistent with the colors that are shown in Figure 2. Scanning electron microscopy was used to image the particle order of the dried crystalline samples. Images collected using a flat specimen mount show the hexagonal arrangement of particles located at the top layer for both the 280 and the 500 mM pS-*co*-NIPAm dried samples (Figure 4, left). The three-dimensional order of the pS-*co*-NIPAm particles is revealed by imaging the sample along cracks or sample cross-sections (Figure 4, middle and right). It is apparent from these images that the samples are well-ordered along the *z*-axis.

To characterize the drying process, in situ reflectance spectroscopy was performed as a drop of the particle suspension was allowed to dry on a glass cover slip.[20] The reflectance probe was positioned at a 90° angle above the drop and about halfway between the center of the drop and

(38) Peiss, C. N. *J. Appl. Phys.* **1989**, *65*, 5235−5237.
(39) Deegan, R. D.; Bakajin, O.; Dupont, T. F.; Huber, G.; Nagel, S. R.; Witten, T. A. *Nature* **1997**, *389*, 827−829.

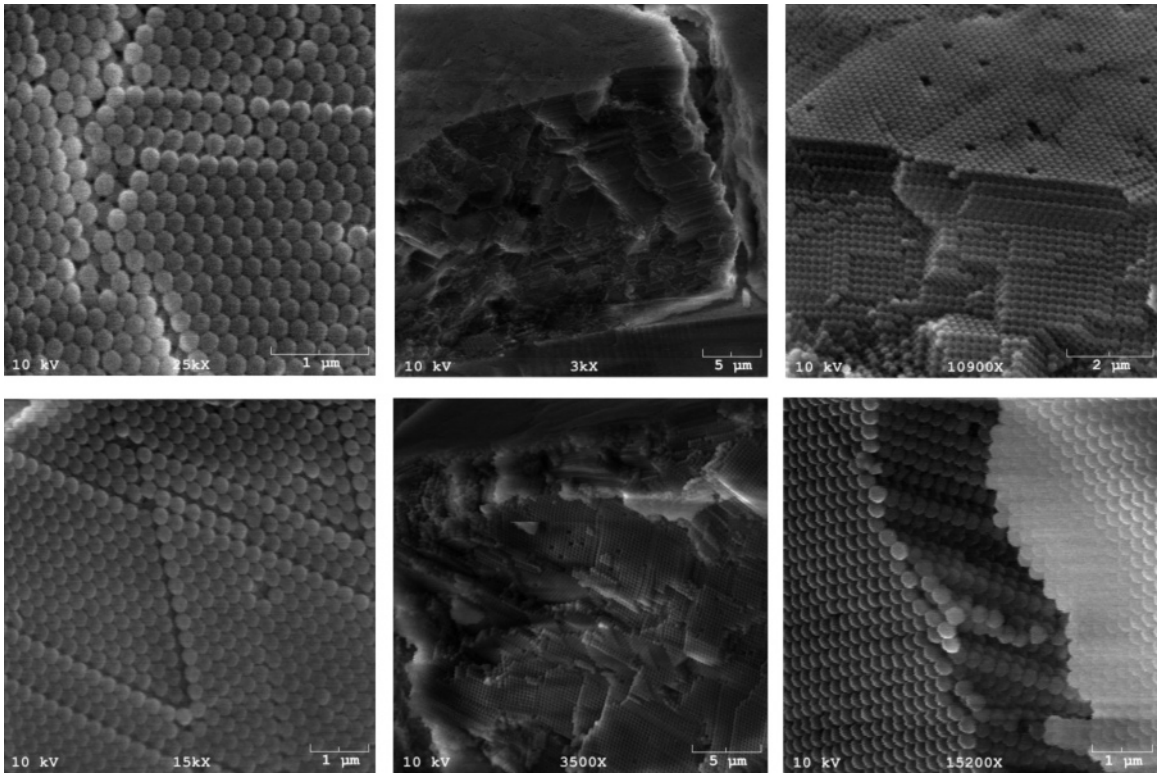


**Figure 4.** Scanning electron microscopy images of 280 mM pS-*co*-NIPAm dried crystals (top row) and 500 mM pS-*co*-NIPAm dried crystals (bottom row). Left: imaging the sample using a flat sample holder. Middle and right: images of crystal cross-sections.

its edge. Reflectance spectra, shown in Figure 5, were collected as the drop dried from the outer edge toward the center of the drop over a time period on the order of minutes. As the sample dries, an initial diffraction peak is observed (at ~495 and ~725 nm for 280 and 500 mM pS-*co*-NIPAm samples, respectively) that is red-shifted as compared to the diffraction peak that was observed for the completely dried samples shown in Figure 3. The intensity of this initial peak increases and becomes blue-shifted over time (during evaporation). A second peak then appears, first as a shoulder to the blue side of the first peak, followed by an increase in intensity as the intensity of the first peak decreases. The intensity of this second, higher energy peak becomes stable once the sample has fully dried, maintaining a final diffraction wavelength that is consistent with the reflectance spectra of the completely dried samples. The colors of the spectra shown in Figure 5 correspond to different times throughout the drying process, which occurred on the order of minutes. Arrows indicate the peaks that decrease and increase with intensity over time.

## Discussion

To characterize the final colloidal crystal product that is formed from suspensions of pS-*co*-NIPAm particles, the properties of the constituent particles were first examined. Variations of the total monomer concentrations used in the synthesis of pS-*co*-NIPAm particles were found to affect the final particle size, as demonstrated using PCS and MALLS characterization tools (Table 1). These light scattering data demonstrate the narrow size distribution for these samples, which is essential for the assembly of a crystalline lattice using spherical particles. Although the addition of NIPAm could introduce thermoresponsivity, there was no significant decrease in particle size with increasing the temperature (25−40 °C), as determined by PCS (Supporting Information). This result indicates that the low NIPAm concentrations that were used in the particle synthesis do not contribute to particle thermoresponsivity, yielding a particle that has a nearly temperature-independent equilibrium swelling volume. As described previously, soft spheres (e.g., pNIPAm particles) cannot maintain crystalline order following drying, thus the rigidity of the pS copolymer spheres affords particle stability throughout the drying process.

Additional information about the particle morphology can be obtained by comparing the ratio of $R_g$ to $R_h$; a sphere of uniform density exhibits an $R_g/R_h$ value of 0.775.[40] The 280 and 500 mM pS-*co*-NIPAm particles demonstrate $R_g/R_h$ values equal to 0.631 and 0.782, respectively, which suggests that these particles possess a polymer composition that is similar to that of a uniform sphere. Differences in the $R_g/R_h$ values may be indicative of variations in the arrangement of the copolymer composition throughout the particle due to the differences in the monomer feed concentration and hence the rate of polymerization. However, it is more likely that the slight increase in NIPAm feed in the 280 mM particle synthesis (26 vs 24% for the 500 mM feed) leads to an increase in the hydrophilicity of the particle surface and hence a more swollen particle periphery. This would lead to the observed $R_g/R_h$ value being lower than the value expected for a uniform sphere.

Figure 1 shows images of both sets of particles acquired using TEM. Similar images were used to determine the pS-

(40) Wyatt, P. J. *Anal. Chim. Acta* **1993**, *272*, 1−40.

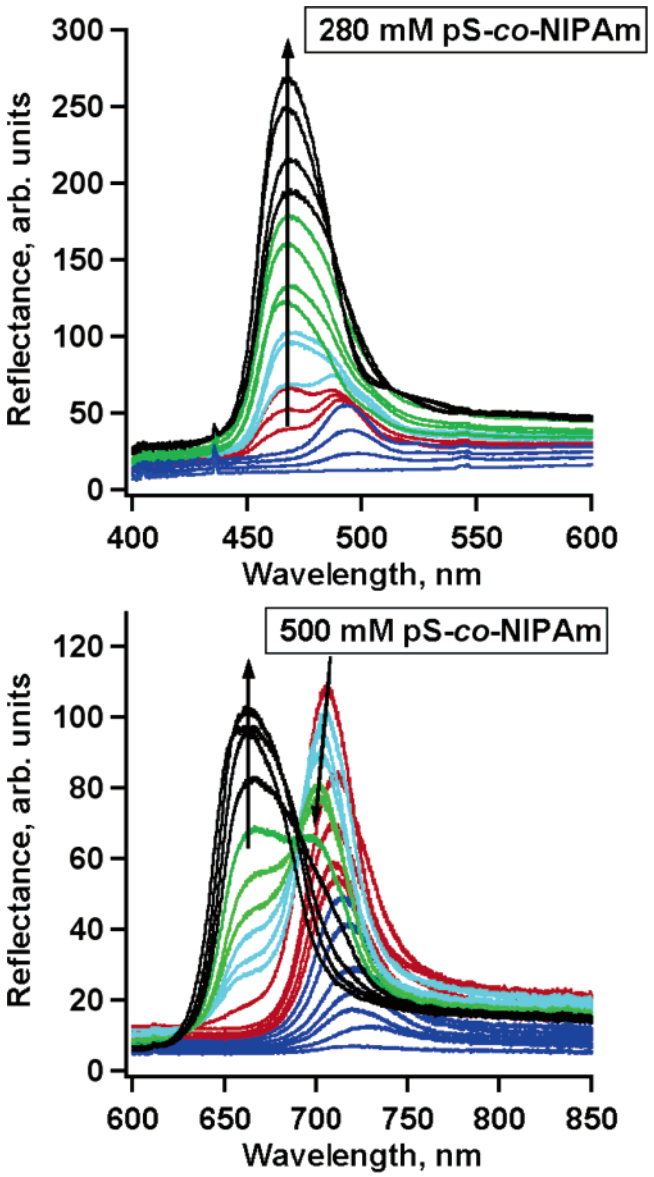


**Figure 5.** In situ reflectance spectra of 280 mM (top) and 500 mM (bottom) pS-*co*-NIPAm particles collected during sample drying over time on the order of ~5 min. The curves correspond to the onset of diffraction, the continuous blue-shift of this diffraction, and the emergence and final diffraction stabilization due to crystals composed of completely dried particles. (Angle of incidence = 90°). In both panels, the line colors indicate the spectral changes with time (blue: initial spectra and red, cyan, green, and black: final spectra).

*co*-NIPAm particle size in its dried state, as listed in Table 1. A significant decrease in particle size is observed as compared to the swollen, hydrated size measured using light scattering. Relative to the diameters found in aqueous media, these sizes correspond to volume decreases of 61.4 and 40.1% for the 280 and 500 mM pS-*co*-NIPAm particles, respectively. It is difficult to estimate the arrangement of the homopolymer-rich regions of the particle based on the reactivity ratios of styrene and NIPAm alone because of the relative hydrophilicity and hydrophobicity of the polymers. However, it has been shown in the literature that the exterior of the pS-*co*-NIPAm particles is composed mostly of the more hydrophilic pNIPAm due to some degree of phase separation, while the center of the particle consists of the more hydrophobic polystyrene.[28,34,41,42] Therefore, it is proposed that this change in size is due primarily to the loss of water from the hydrated pNIPAm-rich periphery of the particle, while the spherical shape is effectively preserved as a result of the dense pS-rich core. This variation in size indicates the extent of surface flexibility that can be realized with these copolymer particles.

The 500 mM pS-*co*-NIPAm particles exhibit a less dramatic reduction in size, which may be due to dissimilarities in the overall copolymer composition and/or distribution as compared to that of the 280 mM pS-*co*-NIPAm particles, thus influencing particle "softness" by affecting the polymer density profile. Since the 280 mM particles possess a slightly larger percentage of NIPAm as well as a smaller $R_g/R_h$ ratio, one might expect the smaller particles to be slightly more hydrated. Indeed, we find that the ratio of hydrated to dry volumes agrees at least semiquantitatively with the measured $R_g/R_h$ ratios for the two sets of particles.[40] Further polymer characterizations are necessary to develop a more detailed understanding of these copolymer particle morphologies.

Despite differences in the apparent degree of "softness" of the particles, the TEM images suggest that there is an adhesive interaction at the interface of the particles where the edges appear to become conjoined. When pS-*co*-NIPAm particles are in contact with a limited number of neighboring particles, they do not appear to be absolutely spherical but appear to be stretched in the direction of the connecting particles (Figure 1B). This effect can also be seen by observing the position of the dark (electron dense) regions located near the center of the particles——the electron contrast is redistributed in a manner that is consistent with the lower electron density material being pulled toward the nearest neighbors. However, a particle that is entirely surrounded by other particles appears to be stretched equally in all directions, sustaining particle uniformity (center particle of Figure 1A). A more concentrated particle array demonstrates a marked difference in particle shape due to the compression of the particles (Figure 1C). This structure is analogous to the features that have been observed with crystals composed of hard spheres that have been sintered by means of thermal annealing techniques.[43−45] As these pS-*co*-NIPAm particles dry and progress into closer contact, they appear to adopt this conformation spontaneously due to the flexibility and adhesiveness of their soft interfaces. This adhesive property may be an effect of interpenetration of the swollen polymer networks during the drying process. This attribute seems to facilitate the stability of their final configuration (vide infra).

Dried colloidal crystals can be achieved by applying a suspension of pS-*co*-NIPAm particles to a substrate (Figure 2). These particular samples were prepared by spreading a drop of the suspension with a pipet to produce a circular

(41) Pelton, R. H. *J. Polym. Sci. A* **1988**, *26*, 9−18.
(42) Duracher, D.; Sauzedde, F.; Elaissari, A.; Perrin, A.; Pichot, C. *Colloid Polym. Sci.* **1998**, *276*, 219−231.
(43) Gates, B.; Park, S. H.; Xia, Y. *Adv. Mater.* **2000**, *12*, 653−656.
(44) Cho, Y.-S.; Yi, G.-R.; Moon, J. H.; Kim, D.-C.; Lee, B.-J.; Yang, S.-M. *Langmuir* **2005**, *21*, 10770−10775.
(45) Sun, Z. Q.; Chen, X.; Zhang, J. H.; Chen, Z. M.; Zhang, K.; Yan, X.; Wang, Y. F.; Yu, W. Z.; Yang, B. *Langmuir* **2005**, *21*, 8987−8991.

pattern. However, other deliberate patterns could be prepared by simply using the pipet to spread the suspension in different directions along the glass substrate, demonstrating the unique ability to use suspensions of these particles as "paint-on" photonic inks (i.e., see the Table of Contents graphic). Particle self-assembly occurs based on the simple process of solvent evaporation, which forces the particles into close contact such that they adopt an organized packing arrangement. Images of the cross-sections of these dried crystals acquired using SEM demonstrate the good 3-D order that exists across the sample thickness (Figure 4). Cracks were found throughout the span of the dried crystal (Figure 4, bottom right), which are typically observed in colloidal crystals as result of the volume reduction associated with sphere shrinkage. However, these cracks do not greatly impact the long-range uniformity of the optical properties of the crystals. The 3-D uniformity of the crystals, as observed at both cracks and cross-sections, demonstrates the remarkable effectiveness of the adhesive qualities of these particles. These soft particle exteriors not only assist in crystalline stability during the drying process by sustaining the position of particles, but they also stabilize the entire crystalline medium in their final configuration, as evidenced by the excellent packing along the *z*-direction.

The close-packed particles located at the top of the dried crystals (Figure 4, left) demonstrate a hexagonal arrangement corresponding to a (111) crystalline plane, which persists across the entire top of these samples. The (111) plane is indicative of face-centered cubic (fcc), hexagonally close-packed (hcp), or randomly stacked structures. This order may be due to particle arrangement along the air−liquid interface during drying or by templating effects perpetuated throughout the thickness of the sample due to the plane of the glass substrate. However, it is difficult to use these SEM images to determine the exact crystalline structure and the extent of the structured layers.[11] Such an arrangement of spherical particles can exhibit Bragg diffraction,[27] and optical spectroscopy is essential to demonstrate the uniformity of crystalline order, which is apparent given the observation of a uniform diffraction color across the length of the sample by visual inspection.

Figure 3 shows the Bragg reflectance peaks for each crystal. The symmetry and breadth of each peak demonstrates the uniformity of crystalline order, and the lack of additional peaks confirms the absence of gross polycrystallinity in these samples, which is sometimes observed with hard sphere crystal systems. A higher scattering background is observed for the crystal composed of the 280 mM pS-*co*-NIPAm particles as compared to the crystal formed with the 500 mM pS-*co*-NIPAm particles. This observation suggests that the former sample possesses a lower crystalline quality, which may be a result of a higher degree of flexibility of the 280 mM pS-co-NIPAm particles (due to their more pronounced hydrated character) that may increase the occurrence of structural defects.

We can characterize these dried crystalline assemblies more fully by comparing the effective refractive index of each sample by using the diffraction wavelengths and crystalline lattice properties, assuming that both dried samples possess a fcc crystalline structure, which is the most common structure for crystals composed of spheres. Bragg's law tells us that

$$m\lambda = 2nd \sin \theta \tag{1}$$

where $\lambda$ is the diffracted wavelength, $m$ is the diffraction order, $n$ is the effective refractive index of the medium, $d$ is the lattice spacing, and $\theta$ is the angle of incidence relative to the lattice plane.[27] Since $d$ is related to the particle diameter ($D$) by

$$d_{hkl} = (1.414D)/(h^2 + k^2 + l^2)^{1/2} \tag{2}$$

where $h$, $k$, and $l$ represent the Miller indices, an approximate refractive index can be determined assuming that the (111) plane is interrogated at near-normal incidence. On the basis of the spectral data, the dried particle sizes from TEM, and the apparent lattice constants from SEM, the dried crystals possess effective refractive indices of 1.41 and 1.49 using 280 and 500 mM pS-*co*-NIPAm particles, respectively. These differences may correspond to subtle differences in the pS-*co*-NIPAm polymer compositions of the two particles.

In situ reflectance measurements were used to elucidate the process of crystalline self-assembly during drying (Figure 5). During this drying process, the pS-*co*-NIPAm particles come into close contact so as to form an ordered structure as the solvent evaporates. The observation of the initial peak for both samples is designated as the point in time at which the particle concentration reaches the minimum volume fraction necessary for entropically driven colloidal crystallization (~0.5 volume fraction).[26,27] The position of this peak suggests that the particles are considerably hydrated relative to their completely dried state. Because a wide area of the sample is interrogated using this reflectance probe, the coexistence of multiple peaks is observed at certain points during the drying process. The continual changes in these diffraction curves, as depicted by curves of different colors over time in Figure 5, suggest that these samples consist of crystals that possess a range of lattice planes along this drying zone that are composed of ordered particles that possess a range of sizes due to partial dehydration. Upon further inspection, another observation can be made with respect to the differences in the intensity of the first peak as compared to the intensity of the final peak for both crystal samples. While the intensity of the initial peak nearly equals the intensity of the final peak for the crystal composed of 500 mM pS-*co*-NIPAm particles, the initial reflectance peak for the 280 mM pS-*co*-NIPAm particles is of a more moderate intensity. It is also important to note that the interparticle spacing suggested by the initial Bragg peaks (longer wavelength) that are observed during drying do not necessarily match well with the swollen particle sizes obtained by PCS. This is especially true for the 280 mM particles, where the low intensity peak initially observed at 495 nm is blue-shifted relative to what one would predict from the swollen particle diameter of 278 nm. The peak that first appears during the drying of the 500 mM particles matches much better to what would be predicted for ~318 nm diameter particles (see Table 1). It is apparently the case that the 500 mM particles

**Scheme 1. Proposed Mechanism of pS-*co*-NIPAm Particle Self-Assembly**

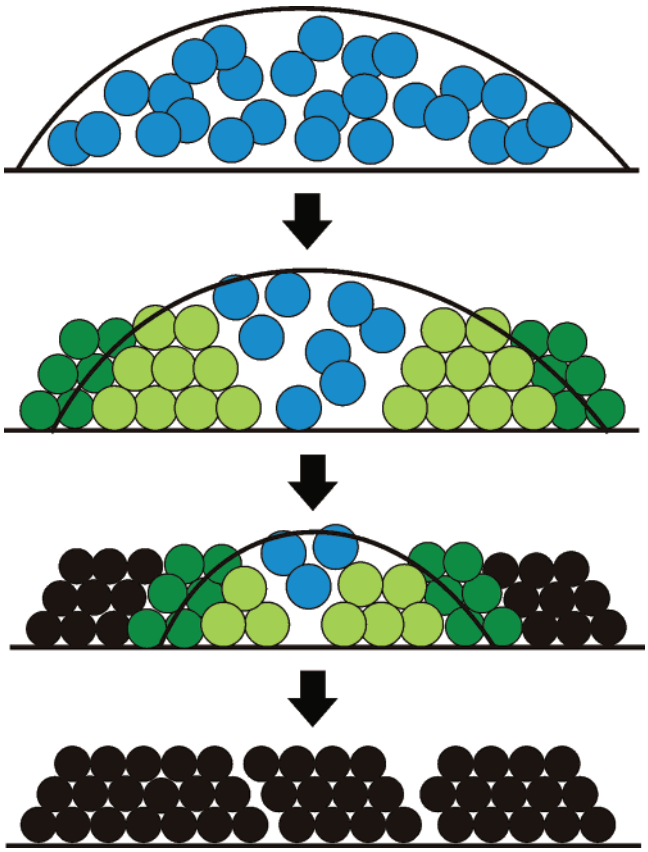

crystallize more readily at low volume fraction. These disparities may be due to variations in the extent of crystal formation during the early stages of drying or differences in the refractive index contrast of the samples during solvent evaporation. Since the exact polymer composition is not known, variations in the particle morphology during the drying process may also contribute to spectral differences between the two types of samples. Additionally, although the presence of two predominant diffraction peaks during drying indicates two different types of ordered states, it is difficult to ascertain the exact crystal lattice constants since there are continuous changes in the particle size (which decreases, due to the loss of water and particle deformation/compression) and the effective refractive index (which increases, due to the loss of water and an increase in the polymer density) during this evolution.

On the basis of the in situ reflectance experiments, a proposed mechanism for the crystallization of the pS-*co*-NIPAm particles is illustrated in Scheme 1. Particles in the suspension initially exist in their fully hydrated state, moving freely in solution (blue circles). As the solvent evaporates, the pS-*co*-NIPAm particles come into close contact so as to form an ordered structure (large, light green circles), and an initial diffraction peak emerges. In the case of the 500 mM particles, the particles may be almost fully hydrated at this stage, maintaining a size approximating the hydrodynamic size determined by PCS. In the case of the 280 mM particles, the particles are probably slightly smaller than the hydrodynamic size determined by PCS (vide supra). As the suspension dries from the outer edge of the drop toward the center of the drop, the diffraction peak blue-shifts and increases in intensity due to the decrease in particle size and increase in refractive index (small, dark green circles). The onset of the most blue-shifted peak is attributed to crystalline regions comprised of completely dried particles (small black circles) since this final peak increases in intensity with ultimately no variation in wavelength and persists after the drying process is complete.

## Conclusion

We have demonstrated that copolymer particles of pS-*co*-NIPAm can be used to fabricate dried colloidal crystals that exhibit Bragg diffraction; the self-assembly of these particles occurs via simple solvent evaporation. The copolymer composition of these particles affords a degree of particle "softness" that allows for particle ordering by introducing particle flexibility, while also possessing hard sphere qualities that provide final crystalline stability when fully dried. Characterizations of the dried crystals were performed using SEM and reflectance spectroscopy to demonstrate the extent of the crystalline order. In situ reflectance spectroscopy was used to show that hydrated particles initially become ordered, and as they lose water via evaporation, their particle size decreases while the crystalline order is retained. Variations in the synthesis conditions of the particles can be used to alter the structure of the colloidal particles, as well as the optical properties of the final crystal. This simple process of self-assembly can be used to fabricate optical materials by means of this straightforward "paint-on" technique.

**Acknowledgment.** The authors acknowledge financial support from the Office of Naval Research and the ONR DURIP program for this work (N00014-03-1-0225 and N00014-04-1-0488).

**Supporting Information Available:** Photon correlation spectroscopy data showing the hydrodynamic radius of the pS-*co*-NIPAm particles as a function of temperature. This material is available free of charge via the Internet at http://pubs.acs.org.

CM061931Y